Combining microenvironment normalization strategies to improve cancer immunotherapy

Fotios Mpekris[a], Chrysovalantis Voutouri[a], James W. Baish[b], Dan G. Duda[c], Lance L. Munn[c], Triantafyllos Stylianopoulos[a,1], and Rakesh K. Jain[c,1]

[a]Cancer Biophysics Laboratory, Department of Mechanical and Manufacturing Engineering, University of Cyprus, 1678 Nicosia, Cyprus; [b]Department of Biomedical Engineering, Bucknell University, Lewisburg, PA 17837; and [c]Edwin L. Steele Laboratories, Department of Radiation Oncology, Massachusetts General Hospital and Harvard Medical School, Boston, MA 02114

Contributed by Rakesh K. Jain, December 17, 2019 (sent for review November 12, 2019; reviewed by Aleksander S. Popel and Hermann Frieboes)

Advances in immunotherapy have revolutionized the treatment of multiple cancers. Unfortunately, tumors usually have impaired blood perfusion, which limits the delivery of therapeutics and cytotoxic immune cells to tumors and also results in hypoxia—a hallmark of the abnormal tumor microenvironment (TME)—that causes immunosuppression. We proposed that normalization of TME using antiangiogenic drugs and/or mechanotherapeutics can overcome these challenges. Recently, immunotherapy with checkpoint blockers was shown to effectively induce vascular normalization in some types of cancer. Although these therapeutic approaches have been used in combination in preclinical and clinical studies, their combined effects on TME are not fully understood. To identify strategies for improved immunotherapy, we have developed a mathematical framework that incorporates complex interactions among various types of cancer cells, immune cells, stroma, angiogenic molecules, and the vasculature. Model predictions were compared with the data from five previously reported experimental studies. We found that low doses of antiangiogenic treatment improve immunotherapy when the two treatments are administered sequentially, but that high doses are less efficacious because of excessive vessel pruning and hypoxia. Stroma normalization can further increase the efficacy of immunotherapy, and the benefit is additive when combined with vascular normalization. We conclude that vessel functionality dictates the efficacy of immunotherapy, and thus increased tumor perfusion should be investigated as a predictive biomarker of response to immunotherapy.

immunotherapy | vascular function | normalization | anti-angiogenic therapy | mechanotherapeutics

Immunotherapy is now a standard of care for multiple types of cancer (1, 2). Cancer cells are able to evade immune responses by activating negative regulatory pathways, also known as immune checkpoints, that block T-cell priming and activation. The inhibition is mediated in large part by the binding of Programmed Cell Death Protein 1 (PD-1) receptor of T cells to the PD-L1 ligand or the binding of cytotoxic T lymphocyte antigen 4 (CTLA-4) receptor of T cells to the B7 molecules in response to various cytokines, such as interferon-γ (IFNγ) (3). The recent development and Food and Drug Administration approval of anti–PD-1/anti–PD-L1 or anti–CTLA-4 antibodies, known as immune checkpoint blockers (ICBs), enables the inhibition of immune checkpoint pathways, thereby eliciting antitumor clinical responses in a variety of solid cancers (4). ICBs have revolutionized the treatment of cancer and have been approved as monotherapies or in combination with other treatments for more than a dozen malignancies (4). While treatment responses are often durable, only a small fraction of patients receiving anti–PD-1/PD-L1 therapy are "cured," while an estimated 87% of US cancer patients currently do not benefit from ICB monotherapies (5). However, with more than 3,500 ongoing clinical trials for cancer immunotherapy (ClinicalTrials.gov), immunotherapy is expected to change the standard of care in many more cancer types.

The absence of a therapeutic benefit in patients has been attributed to a variety of factors, including the abnormal tumor microenvironment (TME), characterized by dysfunctional blood vessels that hinder the delivery of immunotherapeutic agents and cause immunosuppression (1, 6, 7). Indeed, a spatiotemporal lack of sufficient tumor blood perfusion can result in hypoxia, low pH, and inadequate delivery of medicines, which in turn compromises the efficacy of cancer therapies, including immunotherapy (1, 8, 9). One important consequence is that a hypoxic TME helps cancer cells evade the immune system (1). In particular, hypoperfusion hinders the delivery of immune cells to the tumor site through the vascular system, while hypoxia renders the TME immunosuppressive and attenuates the killing potential of immune effector cells (10, 11). Specifically, hypoxia up-regulates immune checkpoints (11, 12), reprograms tumor-associated macrophages (TAMs) from an immunosupportive M1-like phenotype toward an immunosuppressive M2-like state, and may hinder the

Significance

Immunotherapy has changed the standard of care in cancer treatment, but an estimated 87% of patients currently do not derive long-term benefit from immune checkpoint blocker monotherapy. Therefore, new therapeutic strategies are needed to improve the response rates in patients who are resistant to immune checkpoint inhibition. We have developed a mathematical framework to determine how tumor microenvironment normalization strategies—specifically, vascular and stroma normalization—might improve immunotherapy efficacy. By incorporating complex interactions among various types of cancer cells, immune cells, stromal cells, and the vasculature, as well as physical mechanisms, we provide guidelines for designing effective combinatorial therapeutic strategies and point out areas for future investigation.

Author contributions: J.W.B., D.G.D., L.L.M., T.S., and R.K.J. designed research; F.M. and C.V. performed research; T.S. contributed new reagents/analytic tools; F.M., C.V., J.W.B., D.G.D., L.L.M., T.S., and R.K.J. analyzed data; and F.M., C.V., D.G.D., L.L.M., T.S., and R.K.J. wrote the paper.

Reviewers: A.S.P., Johns Hopkins University School of Medicine; and H.F., University of Louisville.

Competing interest statement: R.K.J. has received honoraria from Amgen and consultant fees from Chugai, Merck, Ophthotech, Pfizer, SPARC, SynDevRx, and XTuit; owns equity in Enlight, Ophthotech, and SynDevRx; and serves on the Boards of Trustees of Tekla Healthcare Investors, Tekla Life Sciences Investors, Tekla Healthcare Opportunities Fund, and Tekla World Healthcare Fund. D.G.D. received consultant fees from Bayer, Simcere, and BMS and research grants from Bayer, Exelixis, and BMS. Neither any reagent nor any funding from these organizations was used in this study.

See online for related content such as Commentaries.

[1]To whom correspondence may be addressed. Email: tstylian@ucy.ac.cy or jain@steele.mgh.harvard.edu.

This article contains supporting information online at https://www.pnas.org/lookup/suppl/doi:10.1073/pnas.1919764117/-/DCSupplemental.

First published February 3, 2020.

maturity, and thus the efficacy, of antigen presentation by dendritic cells (10, 13). In addition, hypoxia and acidity affect the function of T lymphocytes and other immune cells (14–16), whereas hypoperfusion and the dense/stiff TME is a physical barrier to T cell infiltration into the tumor (17, 18). Indeed, increased perfusion has been related to improved ICB response (19).

Tumor perfusion is compromised in part by the compression as well as the tortuosity and hyperpermeability of tumor vessels (20). Vessel compression is a result of mechanical forces accumulated within stroma components of tumors (21–23). Indeed, our previous studies (24–26) showed that inhibiting CXCL12/CXCR4 or angiotensin signaling can target cancer-associated fibroblasts (CAFs) and extracellular collagen and hyaluronan, which in turn alleviates intratumoral forces, decompresses tumor vessels, and improves perfusion as well as the outcome of ICBs. We have referred to this approach as stroma normalization (27–30).

Vessel hyperpermeability and tortuosity can be lowered using judicious doses of antiangiogenic (e.g., anti-vascular endothelial growth factor [anti-VEGF]) agents, which increase pericyte coverage and fortify the immature vessels. This strategy, known as vascular normalization, can improve tumor perfusion and thereby increase oxygen and drug delivery, as well as improve the efficacy of various treatments, including immunotherapy (31–36). As a result, perfusion can be increased within the tumor (37). However, vessel normalization is dose-dependent, and high doses of the anti-angiogenic drug can prune the vessels and reduce perfusion and drug delivery (36, 38). In addition, vascular normalization has a transient effect; prolonged anti-angiogenic treatment can result in excessive vessel pruning. This dose- and time-dependency of vascular normalization results in a "normalization window" within which perfusion is improved (33, 38).

Stroma and vascular normalization improve tumor perfusion and oxygenation and can enhance immune response by skewing TAM polarization toward the M1 phenotype, which is tumoricidal and immunostimulatory (10, 13, 24, 39, 40). This can also result in the activation of dendritic cells, cytotoxic T lymphocytes, and natural killer (NK) cells (39). Furthermore, increased tumor perfusion via vessel normalization improves the function of immune cells, contributing to increased killing of cancer cells, which results in the killing of the more resistant stem cell-like cancer cells (41). It has also been proposed that ICB-induced increases in the ratio of $CD4^+/CD8^+$ T cells may decrease the levels of VEGF and thereby decrease tumor vessel permeability, indirectly inducing vascular normalization (10, 42).

Given these complex interactions among cancer cells, immune cells, stroma, and the tumor vasculature, the prediction of the outcome of combined anti-angiogenic, stroma-normalizing, and immune therapies is not intuitive. We hypothesize that a mathematical model that incorporates the known mechanisms of immune response as well as vascular and stroma normalization can explain the experimental observations reported in the literature and provide guidelines for its optimal use and for future experiments. Systems-level mathematical models for the prediction of anti–CTLA-4 and anti–PD-1/anti-PD-L1 response have been developed previously (43–45); however, they do not account for spatial variation in the TME. Here, based on our previous study (41) and the work of others (46, 47), we developed a continuum mathematical modeling framework to account for interactions among different types of cancer cells, immune cells, tumor blood vessels, oxygen supply, and drug delivery. We build on our previous models (41, 48) by incorporating M1-like and M2-like TAMs; $CD4^+$, $CD8^+$, and regulatory (Tregs) T cells, and vascular and perivascular cells and their reported involvement in immunotherapy response. Furthermore, we take into account the dependence of the functional vasculature on stroma components; the concentration gradients of various proangiogenic molecules, including angiopoietins (Ang1 and Ang2), platelet-derived growth factor (PDGF)-B, VEGF, and CXCL12; and the vascular normalization effect of $CD4^+$ and $CD8^+$ T cells (Fig. 1). We simulate how anti-angiogenic, stroma normalization, and immunotherapy treatments affect model components and compare model predictions with previous experimental studies (19, 24, 26, 36, 49). Furthermore, we use model predictions to provide guidelines for the optimal use of these three strategies and point out the gaps in our understanding.

Results

Validation of Model Predictions with Experimental Studies. To assess the validity of our mathematical model and justify the values of the model parameters (*SI Appendix*, Table S1), we compared model predictions with experimental data from five studies, summarized in Table 1. To compare model predictions with experimental data, all model parameters were kept the same as derived separately from pertinent studies. The sole model parameter that was adjusted to fit the experimental data (19, 24, 26, 36, 49) was k_1, which describes the dependence of cancer cell proliferation on oxygen concentration (*SI Appendix*, Table S2). The value of k_1 was determined so that the predicted final tumor volume matched the experimental value of one of the treatment groups, and it was kept the same for comparison of model predictions against all experimental data from all groups of the same study. Therefore, despite the large number of parameters in the model—which is justified by its degree of comprehensiveness—only one parameter was varied for each study.

In our previous studies (e.g., refs. 24 and 26), stroma normalization was applied to improve perfusion and enhance the efficacy of ICBs (anti–PD-1 and anti–CTLA-4) in murine breast tumors. We incorporated the experimental protocols in our model and compared model predictions with experimental results. We modeled stroma normalization as a decrease in the tumor elastic modulus because a primary effect of the strategy is the softening of the tumor. In addition, anti–PD-1 treatment was modeled as an increase in $CD8^+$ T cells, and anti–CTLA-4 treatment was modeled as a decrease in regulatory T cells (Tregs), in line with the reported effects of these two treatments (50). *SI Appendix*, Table S3 summarizes the model parameters associated with each treatment strategy. To demonstrate the comparison between the dimensionless model parameters and the experimental measurements, the values of the different measured parameters are presented relative to the values of the control group. For the first study (26), model predictions agree well with the data on $CD4^+$ and $CD8^+$ T cells, Tregs, and tumor volume in E0771 breast tumors (Fig. 2*A*) and solid stress, tumor perfusion, IFNγ level, and tumor volume in MCa-M3C breast tumors (Fig. 2*B*). In our model, hypoxia was calculated as the percentage of oxygen concentration below the oxygen level in the peritumoral normal tissue, and tumor perfusion was calculated as the ratio of the tumor functional vascular density to that of the normal tissue. In the second breast cancer study (24), model predictions show good agreement with the data on solid stress, tumor perfusion, hypoxia, and IFNγ levels (Fig. 2*C*).

In another breast cancer study from our laboratory, Huang et al. (36) demonstrated that targeting the tumor vasculature with low vascular-normalizing doses, but not high antivascular doses, results in a more homogeneous distribution of functional tumor vessels. Furthermore, low doses were superior to the high doses in polarizing TAMs from an immune inhibitory M2-like phenotype toward an immune stimulatory M1-like phenotype and in facilitating $CD4^+$ and $CD8^+$ T cell tumor infiltration. We simulated the same experimental protocol to compare model predictions to the results of low- and high-dose anti-VEGF treatments. In our simulations, the effects of different doses of anti-VEGF on endothelial cells and VEGF levels were modeled by changes in the endothelial cell and VEGF degradation rate constants, k^{ec}_{a-vegf} and k^{vegf}_{a-vegf}, respectively (*SI Appendix*, Eqs. **S19** and **S22**), according to experimental studies (51, 52). To facilitate comparisons between the dimensionless model parameters and the experimental

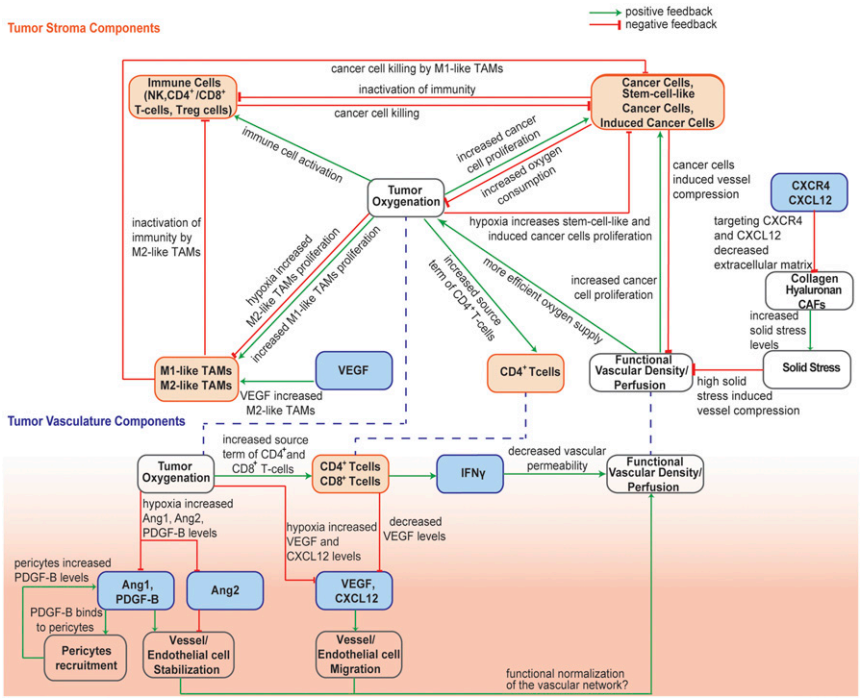

Fig. 1. Schematic of the interactions among model components. The model accounts for various cell populations (orange boxes) and tumor angiogenic factors (blue boxes). TME component: Increases in functional vascular density and tumor perfusion enhance tumor oxygenation. Higher oxygen levels accelerate the proliferation rates of CCs and $CD4^+$ T cells and the activity of immune cells and polarize TAMs from an immune inhibitory M2-like phenotype toward an immune stimulatory M1-like phenotype. Along with the immunostimulatory action of M1-like TAMs, the model accounts for their tumoricidal effect on CCs. According to previous studies, $CD4^+$ T cells stimulate $CD8^+$ T cells, and an increased immune response leads to more efficient killing of all types of cancer cells. Increased proliferation of all cancer cell types results in increased oxygen consumption, inactivation of immune cells, and decreased vessel diameters due to compression-induced hypoxia. Hypoxia favors proliferation of CSCs and ICCs and increases VEGF and CXCL12 levels. In addition, targeting of stroma components through CXCL12/CXCR4 signaling alleviates solid stresses, which are associated with vascular dysfunction. Tumor vasculature component: This initiates angiogenesis through the proliferation and migration of endothelial cells that form the vessels. Angiogenesis is enhanced by high levels of Ang2, which destabilizes vessels, and inhibited by Ang1 and PDGF-B, which recruit pericytes and stabilize vessels. In addition, knockout of $CD4^+$ T cells results in overexpression of VEGF, which is correlated with higher numbers of M2-like TAMs. On the other hand, a decrease in M2-like TAMs results in higher numbers of effector immune cells ($CD8^+$ T cells and NK cells). Increased numbers of $CD4^+$ and $CD8^+$ T cells enhances production rates of IFNγ, which is associated with decreased vessel wall pore size and permeability, leading to vascular normalization. Vascular normalization improves the functionality of the vascular network, leading to an increase in functional vascular density, which enhances cancer cell proliferation.

measurements, the values of the different measured parameters are presented relative to the values of the lowest-dose treatment. Model predictions agree well with our data on tumor perfusion, hypoxia, tumor volume, and the numbers of $CD4^+$ and $CD8^+$ T cells and M1-like TAMs (Fig. 3*A*).

Zheng et al. (19), found that ICBs increased tumor vessel perfusion in the immunotherapy-sensitive E0771 murine breast tumor model, and that the ability of anti–CTLA-4 therapy to increase vessel perfusion was associated with treatment efficacy. Comparisons of model predictions with the data on tumor

Table 1. Experimental studies used to validate model predictions

Cancer type	Main findings	Reference
Breast cancer (E0771; MCA-M3C)	Combination treatment of stroma normalization with immunotherapy increases tumor perfusion, $CD4^+$ and $CD8^+$ T cells, M1-like TAMs, and IFNγ levels and decreases solid stress, hypoxia, and tumor growth rate.	(26)
Breast cancer (MCA-M3C)	Stroma normalization reduces solid stress and hypoxia and enhances tumor perfusion and IFNγ levels.	(24)
Breast cancer (MCAP008)	Low-dose anti-VEGF treatment improves the efficacy of treatment compared with high-dose treatment, by increasing tumor perfusion, $CD4^+$ and $CD8^+$ T cells, and M1-like TAMs and decreasing hypoxia and tumor growth rate.	(36)
Breast cancer (E0771)	Anti–CTLA-4 treatment improves tumor perfusion, oxygenation, and treatment efficacy.	(19)
Hepatocellular carcinoma (RIL-175)	Combination treatment with vascular normalization and immunotherapy increases tumor perfusion and $CD8^+$ T cells and decreases M2-like TAMs and tumor growth rates.	(49)

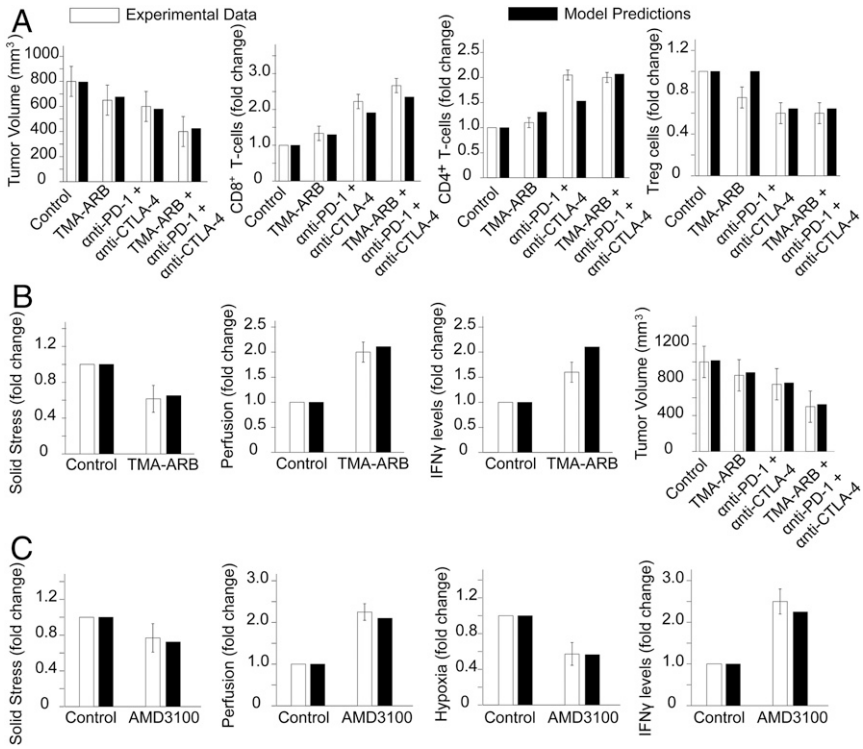

Fig. 2. Comparison of model predictions with experimental data from Chauhan et al. (26) for E0771 (*A*) and MCa-M3C (*B*) breast tumors. (*C*) Comparison of model predictions with experimental data from Chen et al. (24) in MCa-M3C breast tumors. The *x*-axis shows the various treatment groups included in the experimental studies: TMA-ARB, tumor-selective angiotensin receptor blocker; anti–PD-1, PD-1- blocker; anti–CTLA-4, CTLA4- blocker; and AMD3100, a CXCR4 inhibitor.

perfusion, hypoxia, and final volume are presented in Fig. 3*B*. Shigeta et al. (49) demonstrated that dual anti–PD-1/anti–VEGFR-2 (antiangiogenic) therapy has a durable vessel fortification effect in hepatocellular carcinoma (HCC) models and can overcome resistance to antiangiogenic therapy and immunotherapy. Specifically, they found that combination treatment improves efficacy by increasing the fraction of mature vessels, increasing T cell infiltration and activation, and shifting the ratio of M1-like to M2-like TAMs. Model predictions agree well with the data on tumor volume and the fractions of $CD8^+$ T cells and M2-like TAMs (Fig. 3*C*).

Vascular Normalization Improves Immunotherapy if Associated with Increased Perfusion. As mentioned previously, vascular normalization and immunotherapy are two strategies that have been combined for cancer therapy, but the mechanisms of action are not intuitive, and it is difficult to predict a priori the conditions under which the two treatments can be combined favorably. To investigate the effects of different doses of anti-VEGF and immunotherapies, we performed simulations for combinatorial administration of the two treatments. Immunotherapy was modeled as changes in the source term of $CD8^+$ T cells, which is the expected immediate effect of anti–PD-1 treatment and anti-VEGF treatment as an increase in the degradation rate constants of both endothelial cells and VEGF (*SI Appendix*, Table S3). In the model, anti-VEGF treatment was administered first, followed by immunotherapy 4 d later. The anti-VEGF dose was chosen based on experimental data (36). Only low doses of anti-VEGF treatment are effective, because they lead to maintenance of an optimal area of functional vascular density (Fig. 4 and *SI Appendix*, Fig. S1), whereas high doses of anti-VEGF cause excessive vessel pruning, reducing vascular density, perfusion, and treatment efficacy. Temporal and spatial profiles of the values of the model parameters for the sequential administration of anti-VEGF treatment and immunotherapy are presented in Figs. 5 and 6, along with corresponding model predictions for untreated tumors and for immunotherapy alone. Therefore, anti-VEGF treatment is beneficial to immunotherapy only when it is associated with an increase in blood vessel functionality.

Stroma Normalization Enhances the Efficacy of Immunotherapy. We next performed simulations to investigate the effect of stroma normalization on improving the efficacy of immunotherapy. Reduction of stroma components such as CAFs, collagen, and hyaluronan decreases the elastic modulus and alleviates intratumoral stresses, resulting in a "mechanically softer" tumor (28, 29, 53). We investigated the effect of varying the tumor elastic modulus within the range of experimentally measured values (28, 29, 53, 54) on the efficacy of immunotherapy. Low values of the elastic modulus resulted in improved tumor perfusion, increased T-cell infiltration and polarization of TAMs from an immune inhibitory M2-like phenotype toward an immune stimulatory M1-like phenotype, and thus increased cancer cell killing (*SI Appendix*, Figs. S2 and S3). Immunotherapy was again modeled as an increase in the source term of $CD8^+$ T cells. According to our results, higher $CD8^+$ T cell values and lower elastic modulus values are more beneficial. The temporal and spatial distributions of the values of the model parameters are shown in Figs. 5 and 6.

Guided by the foregoing results, we investigated the effect of a triple therapy combining anti-angiogenic, stroma-normalizing, and immune therapy. Given that stroma normalization decompresses tumor blood vessels, it could increase the number of perfused vessels that anti-angiogenic therapy could normalize. Therefore, it is reasonable to hypothesize that combined normalization strategies would further improve perfusion. Indeed,

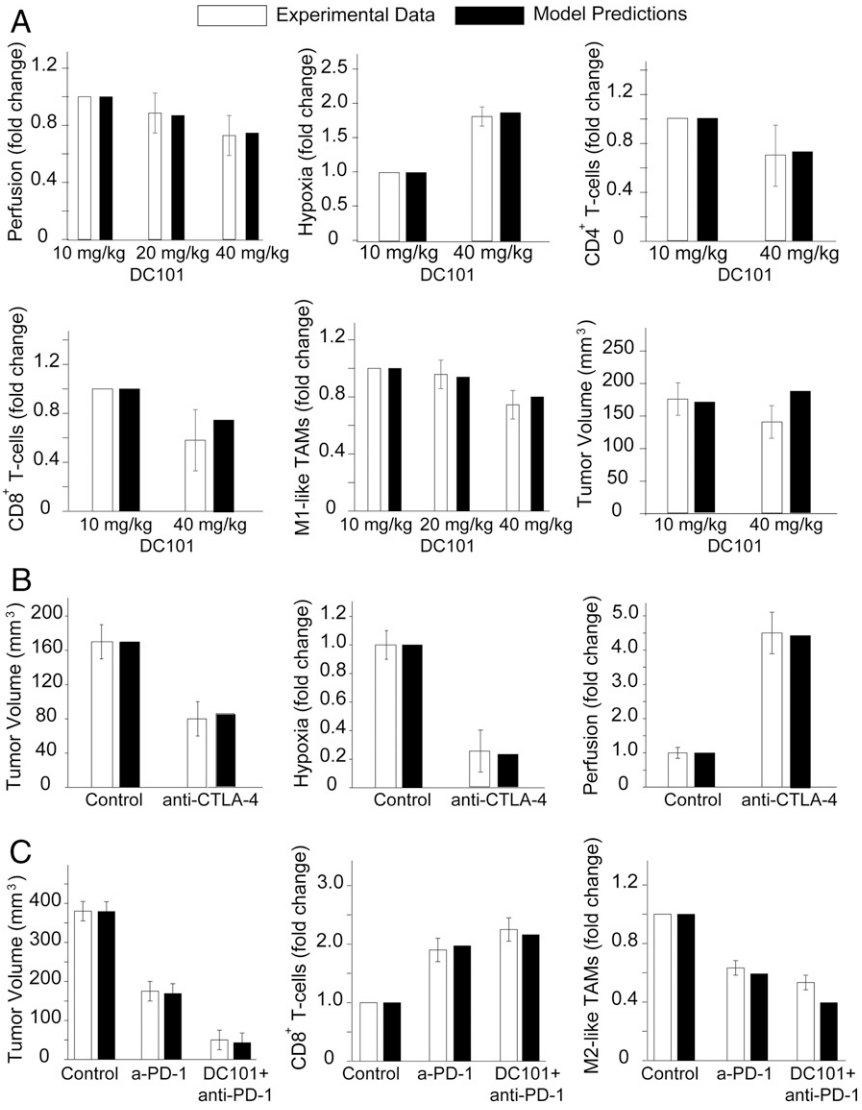

Fig. 3. Comparison of model predictions with experimental data reported by Huang et al. (36) (*A*), Zheng et al. (19) (*B*), and Shigeta et al. (49) (*C*). The *x*-axis shows the various treatment groups included in the experimental studies: DC101, an anti-VEGF antibody; anti–PD-1, a PD-1 blocker; and anti–CTLA-4, a CTLA-4 blocker.

our model predicts that combination of the two strategies with immunotherapy improves functional vascular density and tumor growth delay (*SI Appendix*, Fig. S4).

Sensitivity of Model Predictions to Cancer Cell Proliferation and Migration. Because model predictions can be affected by the proliferation and migration rates of cancer cells, we performed a parametric analysis to assess the sensitivity of our results to these parameters. We varied the values of cancer cell proliferation and migration and repeated simulations for sequential administration of anti-VEGF treatment and immunotherapy (*SI Appendix*, Fig. S5). Model predictions are not sensitive to low values of proliferation and migration. For high proliferation and migration rates, however, the model predicts a reduced efficacy of the combinatorial treatment, which depends mostly on cancer cell proliferation rather than migration.

Discussion

In this study, we have developed a mathematical framework for cancer immunotherapy outcome, accounting for resistance mechanisms mediated by abnormalities in the TME. The model incorporates complex interactions among several types of cancer cells, immune cells, and endothelial cells known to play crucial roles in tumor progression and response to immunotherapy, as well as molecules involved in tumor angiogenesis and anti-angiogenic treatment—processes that have been shown to be modulated by ICB therapy. Our model advances previous studies in that it directly incorporates the effects of immunotherapy on cancer cells as well as on the tumor stroma and vasculature. Specifically, it accounts for M1-like and M2-like TAMs; $CD4^+$, $CD8^+$, and Treg cells; and vascular and perivascular cells, along with many of their reported interactions on immunotherapy response. Furthermore, the model takes into account the dependence of blood vessel functionality on stroma components, the concentration gradients of several proangiogenic molecules (i.e., Ang1, Ang2, PDGF-B, VEGF, and CXCL12), and the vascular normalization effect of $CD4^+$ and $CD8^+$ T cells (Fig. 1). Its increased sophistication is justified by the favorable agreement of the model predictions with a large number of experimental studies. It is clear from the model that immunotherapy efficacy depends on tumor perfusion, and any method for improving perfusion is likely to also enhance immunotherapy (Fig. 7).

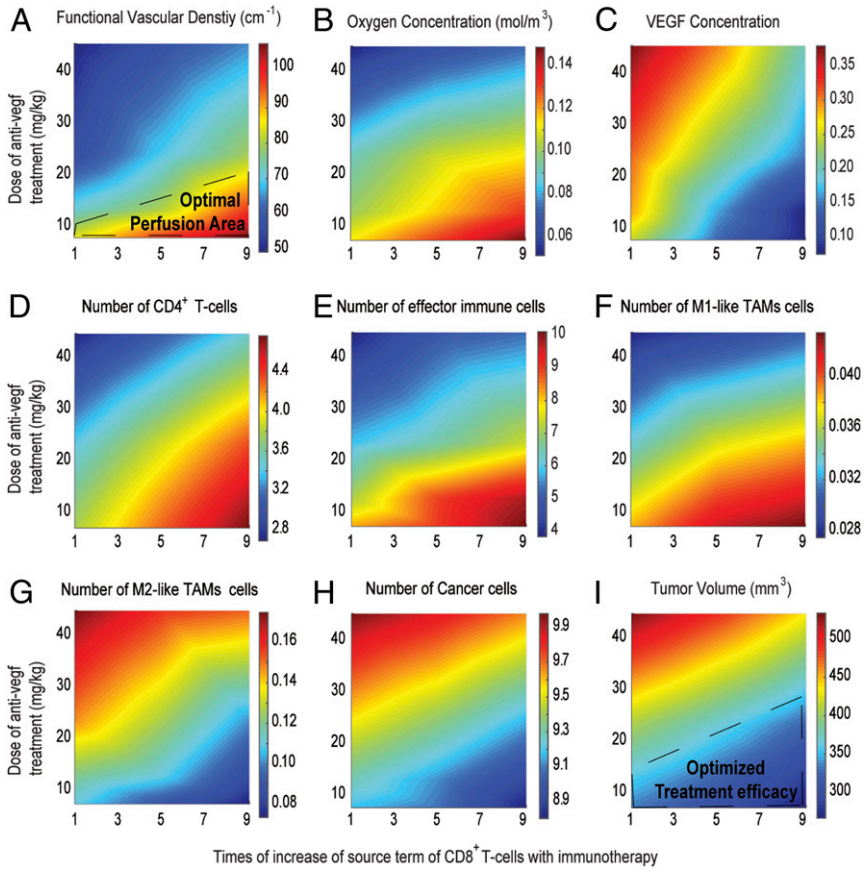

Fig. 4. Effect of different doses of anti-VEGF treatment combined with different values of the source term of CD8$^+$ T cells to model immunotherapy for sequential administration. Shown are phase diagrams for the effect of combinatorial treatment on functional vascular density (*A*), tumor oxygenation (*B*), VEGF level (*C*), CD4$^+$ T cells (*D*), effector immune cells (NK and CD8$^+$ T cells) (*E*) , M1-like (*F*) and M2-like (*G*) TAMs, cancer cell population (*H*), and tumor volume (*I*). Values of model parameters presented in the figure were calculated at the location equidistant from the tumor center and periphery. On the *x*-axis, a value of 1 corresponds to the baseline value of source term of CD8$^+$ T cells (*SI Appendix*, Table S1).

Our study is of particular importance because it proposes new considerations for the use of treatments that normalize the TME. Stroma normalization is beneficial in desmoplastic tumors with abundant compressed vessels, whereas vascular normalization should improve perfusion in tumors with hyperpermeable vessels with open lumens (20). In tumors with both compressed and leaky vessels, the two normalization strategies could be combined to further enhance perfusion. For our theoretical predictions to be implemented in the clinic, we would need to identify the cause of hypoperfusion in each tumor, a challenging task. Although we can make some broad statements (e.g., pancreatic ductal adenocarcinomas are desmoplastic), in many tumors, such as breast cancers, the degree of desmoplasia is highly variable from one tumor subtype to another and potentially from the primary site to the metastatic site. In such cases, the state of an individual tumor should be defined before the selection of an appropriate strategy.

The recent finding that ICB treatment can normalize vessels further encourages its combined use with anti-angiogenic drugs. In fact, the successful recent phase III clinical study for the combined use of the anti–PD-L1 antibody atezolizumab with the anti-VEGFA antibody bevacizumab is consistent with this therapeutic strategy in hepatocellular carcinoma patients (ClinicalTrials.gov Identifier: NCT03434379) (55). The addition of atezolizumab to bevacizumab plus chemotherapy significantly improved overall survival among patients with metastatic nonsquamous non–small-cell lung cancer (56). Furthermore, combinatorial treatment of axitinib with pembrolizumab (57) or with avelumab (58) in patients with advanced renal cell carcinoma increased progression free-survival. Also, the effect of lenvatinib plus pembrolizumab is being investigated in a randomized phase III clinical study, as it was found that this treatment had antitumor activity in patients with advanced recurrent endometrial cancer (59). However, the benefit of anti-angiogenic drugs is time- and dose-dependent, and identifying the normalization window of a tumor is challenging. Our model predictions are further validated by recent clinical trials showing that combination treatment with a low dose of an anti-angiogenic agent (regorafenib) with nivolumab is superior to high doses in advanced gastric or colorectal cancer (60). Our model suggests that administration of immunotherapy with anti-angiogenic treatment could protect blood vessels from excessive pruning (49). However, the extent of ICB-induced normalization is likely to vary with tumor type, stage of disease, and location, and it might not even occur in some tumor types. We should also emphasize that for the results presented in Figs. 4–6, we modeled vascular normalization considering only inhibition of VEGF. Normalization of tumor blood vessels can be also achieved with the use of tyrosine kinase inhibitors (TKIs), which target other proangiogenic pathways besides VEGF, such as PDGF receptors on pericytes. Inhibiting pericytes, and thus vessel maturation, would lessen the impact of any anti-VEGF effect and thus interfere with ICB-induced normalization (61).

The identification of tumor perfusion as a key parameter for the efficacy of immunotherapy also highlights the potential use of perfusion measures as markers for immunotherapy prediction

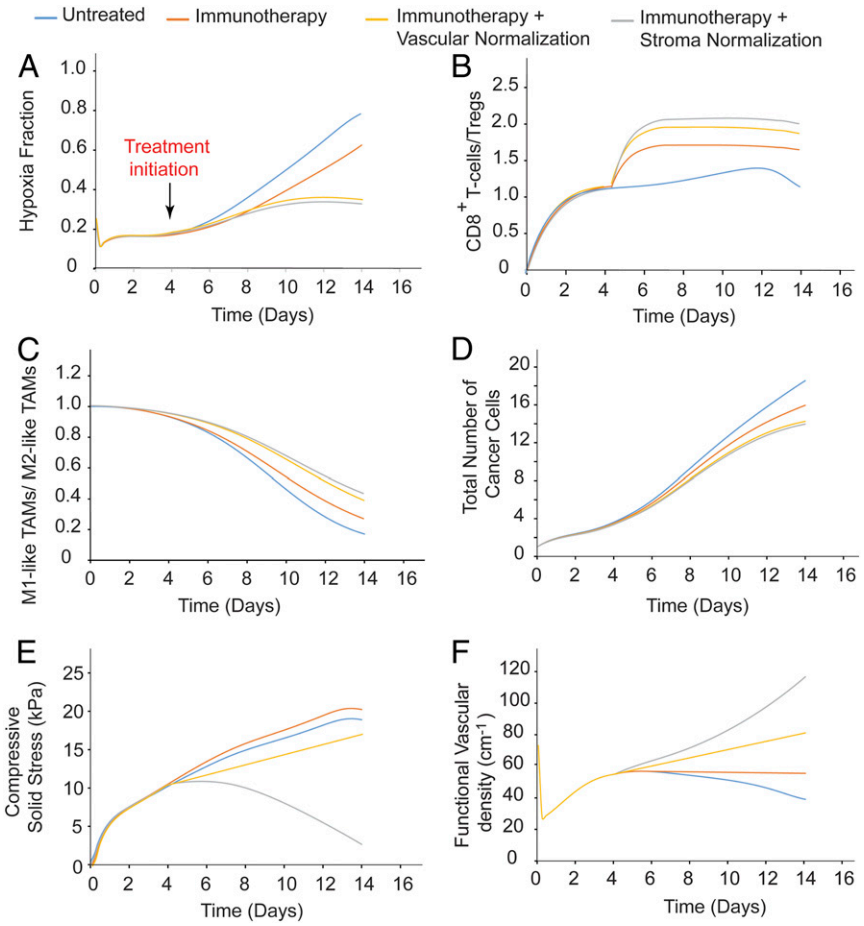

Fig. 5. Temporal distribution of the values of model parameters: hypoxia fraction (*A*), ratio of $CD8^+$ T cells to Tregs (*B*), ratio of M1-like to M2-like TAMs (*C*), cancer cell population (*D*), solid stress (*E*) and functional vascular density (*F*), calculated at the center of the tumor for untreated tumors and tumors receiving immunotherapy alone or combined with a normalization treatment.

(62). To date, there are no universal predictive biomarkers for ICBs. Biomarkers based on the expression of PD-L1, have been proposed only for certain tumor types (63). However, some tumors respond even when PD-L1 expression is low, and others do not respond even when PD-L1 expression is elevated. In addition, a clinical study found that anti–CTLA-4 immunotherapy does not deplete regulatory T cells (64). Tumor types might have a significantly different immunologic background, and thus the identification of common predictive markers based on molecular information is extremely challenging (7). On the other hand, tumor perfusion can be measured in patients and should be tested as a biomarker in prospective trials.

Our model has certain limitations, including the fact that it accounts only for a subset of immune cells of the TME (NK cells, $CD8^+/CD4^+$ T cells, Tregs, M1/M2-like TAMs) and for a subset of angiogenic molecules (Ang1, Ang2, PDGF-B, VEGF, and CXCL12). Other types of immune cells involved in the cancer-immunity cycle (e.g., dendritic cells) and other molecules (e.g.,

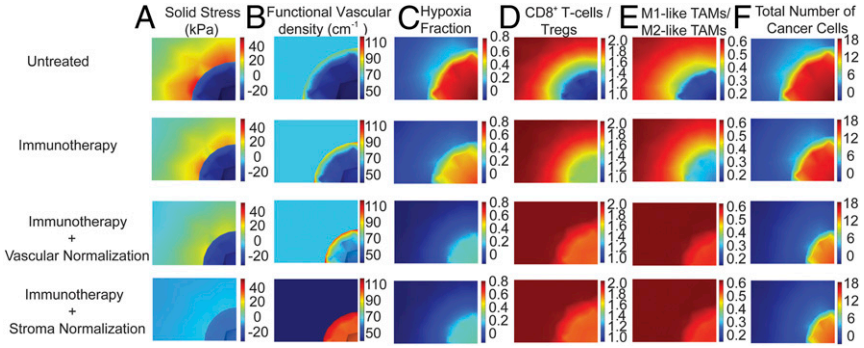

Fig. 6. Spatial distribution of the values of model parameters: solid stress (*A*), functionalvascular density (*B*), hypoxia fraction (*C*), ratio of $CD8^+$ T cells to Tregs (*D*), ratio of M1-like to M2-like TAMs (*E*), cancer cell population (*F*) for untreated tumors and tumors receiving immunotherapy alone or combined with a normalization treatment.

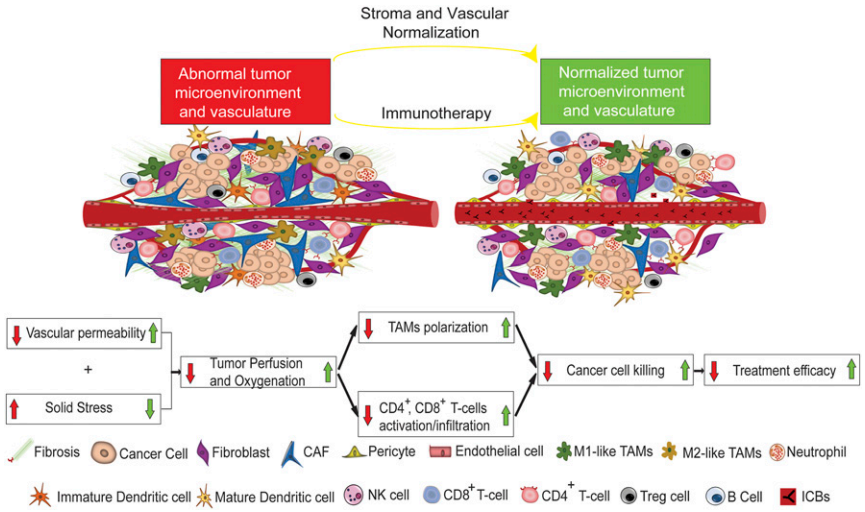

Fig. 7. Schematic of proposed mechanism of action of normalization strategies to improve immunotherapy. (Adapted with permission from ref. 7.) Combined administration of immunotherapy with stroma and/or vascular normalization restores vascular functionality and alleviates solid stress, leading to improved tumor perfusion and oxygenation, skewing TAM polarization away from the immunosuppressive M2-like phenotype to the M1-like phenotype, stimulating immunity (e.g., $CD4^+$ and $CD8^+$ T cells) and thus increasing cancer cell killing.

hypoxia-inducible factor 1, transforming growth factor [TGF-β], and interleukins) that influence treatment outcome (3) are not considered. In particular, TGF-β, which is a target molecule of stroma normalization, can affect immunotherapy through many mechanisms, such as the intratumoral distribution of T cells (18, 65). Indeed, stroma-normalizing mechanotherapeutic drugs might have the capacity to directly act on immune and endothelial cells (66–68). Another process not included in the model is the delivery of ICB antibodies from the bloodstream into the tumor; instead, we model their activity, the lack of dependence of T-cell infiltration from VEGF levels, and the repulsion of T cells from cancer cells via CXCR4 signaling, and we assume that migration rates of T cells do not depend on oxygen levels. High VEGF levels reduce the expression of adhesion molecules in the endothelial cell lining of the tumor vessel walls, which limits the ability of T cells to adhere and infiltrate into the tumor (1, 69), and T cells move faster under normal tissue oxygenation. In addition, the production of VEGF from stroma cells (i.e., fibroblasts and immune cells) is not included (70). Furthermore, the model does not account for adhesion and extravasation of T cells, or the fact that IFNγ, apart from normalizing the vessel wall, can also cause vessel pruning (71, 72). We also did not include lymphatic vessels, which play an important role in the immune response (1). Finally, calculating a partial rank correlation coefficient for the sensitivity of the solution to various model parameters can potentially improve the fidelity of the model when individual simulations can be run much faster than currently feasible (~24 h per simulation; *SI Appendix*) (44, 73).

Nevertheless, the model is relatively comprehensive and reproduces complex, rich behaviors. It includes a large number of parameters associated with the interactions of cancer, immune, and endothelial cells and angiogenic molecules, as well as physiological and mechanical tumor properties (*SI Appendix*, Table S1). Baseline values of the model parameters were determined independently using data from the literature. Accordingly, model predictions are in good qualitative agreement with a large set of independent experimental data and could serve as a foundation for further experimental studies to examine the link between normalization treatments and immunotherapy.

Materials and Methods

Description of the Mathematical Model. A schematic of the tumor components incorporated into the model and their interrelations is provided in Fig. 1, and a detailed presentation of the model equations and assumptions is given in *SI Appendix*. The model accounts for three types of cancer cells: cancer cells (CCs), stem-like cancer cells (CSCs), and induced cancer cells (ICCs). It also includes cells of the immune system, including TAMs and the tumor vasculature, as described in Fig. 1 and detailed in *SI Appendix*. In our model, tumor growth is determined by the combined proliferation of all cancer cells. The population balance of CCs, CSCs, and ICCs depends on tumor perfusion and oxygenation. The proliferation rate of CCs increases with increasing oxygen level, while the proliferation rates of CSCs and ICCs increase under hypoxic conditions (41, 74). Other events that determine the population of cancer cells are their killing by effector immune cells and M1-like TAMs (47, 75) and the interconversion among CCs, CSCs, and ICSs.

Proliferation of all cancer cells leads to a decrease in vessel diameter due to compression of tumor vessels (21). The functional vascular density depends on the hyperpermeability of blood vessels, the compression of blood vessels by cancer cells and solid stress levels, and the density of endothelial cells. According to previous experimental findings, IFNγ concentration affects vessel permeability; specifically, elimination of immune $CD4^+$ T cells and $CD8^+$ T cells leads to a decrease in IFNγ, which in turn increases vessel wall pore size and vessel permeability by fivefold (42, 76). Endothelial cell concentration depends on levels of tumor angiogenic factors. Several molecules have been shown to affect the tumor vasculature, including Ang1 and Ang2, PDGF-B, VEGF, and CXCL12. The common feature of all these proteins is that they are overproduced under hypoxic conditions. Ang1 is produced by pericytes, while Ang2 is produced mainly by endothelial cells, and the two have competing effects: Ang1 and PDGF-β have been shown to stabilize endothelial cells, producing mature vessels, while Ang2 has the opposite effect, destabilizing endothelial cells, favoring angiogenesis (77, 78). The effects of Ang1 and Ang2 are context-dependent (79, 80). VEGF and CXCL12 are produced mainly by tumor cells, and they coordinate endothelial cell migration and angiogenesis (81). Furthermore, in our model we account indirectly for stroma normalization via targeting of CXCL12/CXCR4 signaling, which results in decreases of stroma components and thus tumor softening. According to previous studies (28, 29, 53), a dense tumor stroma is associated with high values of elastic modulus and solid stress levels that reduce functional vascular density (82), whereas reduction of stroma decreases the values of the elastic modulus.

We further account for four different types of immune cells: $CD4^+$ T cells, immune effector cells (i.e., NK cells, $CD8^+$ T cells), and Tregs. Our model takes into consideration the growth/death rate of the cells, their inactivation by cancer cells, and their activation by oxygen, which increases their killing potential (41, 75). Furthermore, we account for two different types of TAMs, M1-like and M2-like, whose production rates are associated with oxygen levels, with a decrease in hypoxia skewing TAM polarization away from the M2-like to the M1-like phenotype (33–35). In addition, VEGF overexpression

is correlated with higher numbers of M2-like TAMs (33). M2-like TAMs have been reported to inhibit the number of immune effector cells (NK cells and $CD8^+$ T cells) (39). Transport of oxygen is described by the convection-diffusion reaction equation, and diffusion is the dominant mode of transport for oxygen (82, 83).

Additional details about the model are provided in *SI Appendix*.

Data availability. All data supporting the findings of this study are available in the paper and *SI Appendix*.

Code availability. The COMSOL code is available in *SI Appendix*.

ACKNOWLEDGMENTS. We thank Drs. Zohreh Amoozgar, Meenal Datta, Yuhui Huang and John Martin for their insightful comments on this work. This study was supported by grants from the National Foundation for Cancer Research, the Ludwig Center at Harvard, the Jane's Trust Foundation, the Advanced Medical Research Foundation, the National Cancer Institute (Grants R35 CA197743, R01 CA208205, and U01 CA224173, to R.K.J.), the Research Promotion Foundation of Cyprus (POST-DOC/0718/0084, INFRASTRUCTURE/1216/0052, to T.S.), and a postdoctoral fellowship from the University of Cyprus (to F.M.).

1. L. L. Munn, R. K. Jain, Vascular regulation of antitumor immunity. *Science* **365**, 544–545 (2019).
2. J. Xin Yu, V. M. Hubbard-Lucey, J. Tang, Immuno-oncology drug development goes global. *Nat. Rev. Drug Discov.* **18**, 899–900 (2019).
3. D. S. Chen, I. Mellman, Elements of cancer immunity and the cancer-immune set point. *Nature* **541**, 321–330 (2017).
4. X. Li, W. Song, C. Shao, Y. Shi, W. Han, Emerging predictors of the response to the blockade of immune checkpoints in cancer therapy. *Cell. Mol. Immunol.* **16**, 28–39 (2019).
5. A. Haslam, V. Prasad, Estimation of the percentage of US patients with cancer who are eligible for and respond to checkpoint inhibitor immunotherapy drugs. *JAMA Netw. Open* **2**, e192535 (2019).
6. M. Datta, L. M. Coussens, H. Nishikawa, F. S. Hodi, R. K. Jain, Reprogramming the tumor microenvironment to improve immunotherapy: Emerging strategies and combination therapies. *Am. Soc. Clin. Oncol. Educ. Book* **39**, 165–174 (2019).
7. J. D. Martin, H. Cabral, T. Stylianopoulos, R. K. Jain, Improving cancer immunotherapy using nanomedicines: Progress, opportunities and challenges. *Nat. Rev. Clin. Oncol.*, 10.1038/s41571-019-0308-z (2019).
8. R. K. Jain, T. Stylianopoulos, Delivering nanomedicine to solid tumors. *Nat. Rev. Clin. Oncol.* **7**, 653–664 (2010).
9. T. Stylianopoulos, L. L. Munn, R. K. Jain, Reengineering the physical microenvironment of tumors to improve drug delivery and efficacy: From mathematical modeling to bench to bedside. *Trends Cancer* **4**, 292–319 (2018).
10. Y. Huang, S. Goel, D. G. Duda, D. Fukumura, R. K. Jain, Vascular normalization as an emerging strategy to enhance cancer immunotherapy. *Cancer Res.* **73**, 2943–2948 (2013).
11. M. Z. Noman *et al.*, Hypoxia: A key player in antitumor immune response. A review in the theme: Cellular responses to hypoxia. *Am. J. Physiol. Cell Physiol.* **309**, C569–C579 (2015).
12. M. Z. Noman *et al.*, PD-L1 is a novel direct target of HIF-1α, and its blockade under hypoxia enhanced MDSC-mediated T cell activation. *J. Exp. Med.* **211**, 781–790 (2014).
13. T. E. Peterson *et al.*, Dual inhibition of Ang-2 and VEGF receptors normalizes tumor vasculature and prolongs survival in glioblastoma by altering macrophages. *Proc. Natl. Acad. Sci. U.S.A.* **113**, 4470–4475 (2016).
14. A. Facciabene *et al.*, Tumour hypoxia promotes tolerance and angiogenesis via CCL28 and T(reg) cells. *Nature* **475**, 226–230 (2011).
15. A. Calcinotto *et al.*, Modulation of microenvironment acidity reverses anergy in human and murine tumor-infiltrating T lymphocytes. *Cancer Res.* **72**, 2746–2756 (2012).
16. A. Palazón, J. Aragonés, A. Morales-Kastresana, M. O. de Landázuri, I. Melero, Molecular pathways: Hypoxia response in immune cells fighting or promoting cancer. *Clin. Cancer Res.* **18**, 1207–1213 (2012).
17. H. Salmon *et al.*, Matrix architecture defines the preferential localization and migration of T cells into the stroma of human lung tumors. *J. Clin. Invest.* **122**, 899–910 (2012).
18. S. Mariathasan *et al.*, TGFβ attenuates tumour response to PD-L1 blockade by contributing to exclusion of T cells. *Nature* **554**, 544–548 (2018).
19. X. Zheng *et al.*, Increased vessel perfusion predicts the efficacy of immune checkpoint blockade. *J. Clin. Invest.* **128**, 2104–2115 (2018).
20. T. Stylianopoulos, R. K. Jain, Combining two strategies to improve perfusion and drug delivery in solid tumors. *Proc. Natl. Acad. Sci. U.S.A.* **110**, 18632–18637 (2013).
21. G. Griffon-Etienne, Y. Boucher, C. Brekken, H. D. Suit, R. K. Jain, Taxane-induced apoptosis decompresses blood vessels and lowers interstitial fluid pressure in solid tumors: Clinical implications. *Cancer Res.* **59**, 3776–3782 (1999).
22. T. P. Padera *et al.*, Pathology: Cancer cells compress intratumour vessels. *Nature* **427**, 695 (2004).
23. T. Stylianopoulos *et al.*, Causes, consequences, and remedies for growth-induced solid stress in murine and human tumors. *Proc. Natl. Acad. Sci. U.S.A.* **109**, 15101–15108 (2012).
24. I. X. Chen *et al.*, Blocking CXCR4 alleviates desmoplasia, increases T-lymphocyte infiltration, and improves immunotherapy in metastatic breast cancer. *Proc. Natl. Acad. Sci. U.S.A.* **116**, 4558–4566 (2019).
25. M. Pinter, R. K. Jain, Targeting the renin-angiotensin system to improve cancer treatment: Implications for immunotherapy. *Sci. Transl. Med.* **9**, eaan5616 (2017).
26. V. P. Chauhan *et al.*, Reprogramming the microenvironment with tumor-selective angiotensin blockers enhances cancer immunotherapy. *Proc. Natl. Acad. Sci. U.S.A.* **116**, 10674–10680 (2019).
27. V. P. Chauhan *et al.*, Angiotensin inhibition enhances drug delivery and potentiates chemotherapy by decompressing tumour blood vessels. *Nat. Commun.* **4**, 2516 (2013).
28. P. Papageorgis *et al.*, Tranilast-induced stress alleviation in solid tumors improves the efficacy of chemo- and nanotherapeutics in a size-independent manner. *Sci. Rep.* **7**, 46140 (2017).
29. C. Polydorou, F. Mpekris, P. Papageorgis, C. Voutouri, T. Stylianopoulos, Pirfenidone normalizes the tumor microenvironment to improve chemotherapy. *Oncotarget* **8**, 24506–24517 (2017).
30. Y. Zhao *et al.*, Losartan treatment enhances chemotherapy efficacy and reduces ascites in ovarian cancer models by normalizing the tumor stroma. *Proc. Natl. Acad. Sci. U.S.A.* **116**, 2210–2219 (2019).
31. R. K. Jain, Determinants of tumor blood flow: A review. *Cancer Res.* **48**, 2641–2658 (1988).
32. R. K. Jain, Normalizing tumor vasculature with anti-angiogenic therapy: A new paradigm for combination therapy. *Nat. Med.* **7**, 987–989 (2001).
33. R. K. Jain, Normalization of tumor vasculature: An emerging concept in anti-angiogenic therapy. *Science* **307**, 58–62 (2005).
34. S. Goel *et al.*, Normalization of the vasculature for treatment of cancer and other diseases. *Physiol. Rev.* **91**, 1071–1121 (2011).
35. S. Goel, D. Fukumura, R. K. Jain, Normalization of the tumor vasculature through oncogenic inhibition: An emerging paradigm in tumor biology. *Proc. Natl. Acad. Sci. U.S.A.* **109**, E1214 (2012).
36. Y. Huang *et al.*, Vascular normalizing doses of antiangiogenic treatment reprogram the immunosuppressive tumor microenvironment and enhance immunotherapy. *Proc. Natl. Acad. Sci. U.S.A.* **109**, 17561–17566 (2012).
37. R. K. Jain, Antiangiogenesis strategies revisited: From starving tumors to alleviating hypoxia. *Cancer Cell* **26**, 605–622 (2014).
38. R. K. Jain, Normalizing tumor microenvironment to treat cancer: Bench to bedside to biomarkers. *J. Clin. Oncol.* **31**, 2205–2218 (2013).
39. C. Rolny *et al.*, HRG inhibits tumor growth and metastasis by inducing macrophage polarization and vessel normalization through downregulation of PlGF. *Cancer Cell* **19**, 31–44 (2011).
40. J. Kloepper *et al.*, Ang-2/VEGF bispecific antibody reprograms macrophages and resident microglia to anti-tumor phenotype and prolongs glioblastoma survival. *Proc. Natl. Acad. Sci. U.S.A.* **113**, 4476–4481 (2016).
41. F. Mpekris, J. W. Baish, T. Stylianopoulos, R. K. Jain, Role of vascular normalization in benefit from metronomic chemotherapy. *Proc. Natl. Acad. Sci. U.S.A.* **114**, 1994–1999 (2017).
42. L. Tian *et al.*, Mutual regulation of tumour vessel normalization and immunostimulatory reprogramming. *Nature* **544**, 250–254 (2017).
43. O. Milberg *et al.*, A QSP model for predicting clinical responses to monotherapy, combination and sequential therapy following CTLA-4, PD-1, and PD-L1 checkpoint blockade. *Sci. Rep.* **9**, 11286 (2019).
44. M. Jafarnejad *et al.*, A computational model of neoadjuvant PD-1 inhibition in non-small cell lung cancer. *AAPS J.* **21**, 79 (2019).
45. H. Wang *et al.*, In silico simulation of a clinical trial with anti-CTLA-4 and anti-PD-L1 immunotherapies in metastatic breast cancer using a systems pharmacology model. *R. Soc. Open Sci.* **6**, 190366 (2019).
46. G. E. Mahlbacher, K. C. Reihmer, H. B. Frieboes, Mathematical modeling of tumor-immune cell interactions. *J. Theor. Biol.* **469**, 47–60 (2019).
47. G. Mahlbacher, L. T. Curtis, J. Lowengrub, H. B. Frieboes, Mathematical modeling of tumor-associated macrophage interactions with the cancer microenvironment. *J. Immunother. Cancer* **6**, 10 (2018).
48. C. Voutouri *et al.*, Experimental and computational analyses reveal dynamics of tumor vessel cooption and optimal treatment strategies. *Proc. Natl. Acad. Sci. U.S.A.* **116**, 2662–2671 (2019).
49. K. Shigeta *et al.*, Dual PD-1 and VEGFR-2 blockade promotes vascular normalization and enhances anti-tumor immune responses in HCC. *Hepatology*, 10.1002/hep.30889. (2019).
50. S. A. Quezada, K. S. Peggs, M. A. Curran, J. P. Allison, CTLA4 blockade and GM-CSF combination immunotherapy alters the intratumor balance of effector and regulatory T cells. *J. Clin. Invest.* **116**, 1935–1945 (2006).
51. V. Boige *et al.*, Efficacy, safety, and biomarkers of single-agent bevacizumab therapy in patients with advanced hepatocellular carcinoma. *Oncologist* **17**, 1063–1072 (2012).
52. C. G. Willett *et al.*, Direct evidence that the VEGF-specific antibody bevacizumab has antivascular effects in human rectal cancer. *Nat. Med.* **10**, 145–147 (2004).
53. F. Mpekris *et al.*, Sonic-hedgehog pathway inhibition normalizes desmoplastic tumor microenvironment to improve chemo- and nanotherapy. *J. Control. Release* **261**, 105–112 (2017).
54. J. D. Martin *et al.*, Dexamethasone increases cisplatin-loaded nanocarrier delivery and efficacy in metastatic breast cancer by normalizing the tumor microenvironment. *ACS Nano* **13**, 6396–6408 (2019).
55. R. K. Jain, J. Wei, P. M. Gullino, Pharmacokinetics of methotrexate in solid tumors. *J. Pharmacokinet. Biopharm.* **7**, 181–194 (1979).
56. M. A. Socinski *et al.*; IMpower150 Study Group, Atezolizumab for first-line treatment of metastatic nonsquamous NSCLC. *N. Engl. J. Med.* **378**, 2288–2301 (2018).

57. B. I. Rini *et al.*; KEYNOTE-426 Investigators, Pembrolizumab plus axitinib versus sunitinib for advanced renal-cell carcinoma. *N. Engl. J. Med.* **380**, 1116–1127 (2019).
58. R. J. Motzer *et al.*, Avelumab plus axitinib versus sunitinib for advanced renal-cell carcinoma. *N. Engl. J. Med.* **380**, 1103–1115 (2019).
59. V. Makker *et al.*, Lenvatinib plus pembrolizumab in patients with advanced endometrial cancer: An interim analysis of a multicentre, open-label, single-arm, phase 2 trial. *Lancet Oncol.* **20**, 711–718 (2019).
60. S. Fukuoka *et al.*, Regorafenib plus nivolumab in patients with advanced gastric (GC) or colorectal cancer (CRC): An open-label, dose-finding, and dose-expansion phase 1b trial (REGONIVO, EPOC1603). *J. Clin. Oncol.* **37**, 2522 (2019).
61. Y. Chen *et al.*, CXCR4 inhibition in tumor microenvironment facilitates anti-programmed death receptor-1 immunotherapy in sorafenib-treated hepatocellular carcinoma in mice. *Hepatology* **61**, 1591–1602 (2015).
62. J. D. Martin, G. Seano, R. K. Jain, Normalizing function of tumor vessels: Progress, opportunities, and challenges. *Annu. Rev. Physiol.* **81**, 505–534 (2019).
63. S. L. Topalian, J. M. Taube, R. A. Anders, D. M. Pardoll, Mechanism-driven biomarkers to guide immune checkpoint blockade in cancer therapy. *Nat. Rev. Cancer* **16**, 275–287 (2016).
64. A. Sharma *et al.*, Anti-CTLA-4 immunotherapy does not deplete FOXP3(+) regulatory T cells (Tregs) in human cancers. *Clin. Cancer Res.* **25**, 1233–1238 (2019).
65. E. Batlle, J. Massagué, Transforming growth factor-β signaling in immunity and cancer. *Immunity* **50**, 924–940 (2019).
66. D. P. Regan *et al.*, The angiotensin receptor blocker losartan suppresses growth of pulmonary metastases via AT1R-independent inhibition of CCR2 signaling and monocyte recruitment. *J. Immunol.* **202**, 3087–3102 (2019).
67. S. Foulquier *et al.*, The role of receptor MAS in microglia-driven retinal vascular development. *Angiogenesis* **22**, 481–489 (2019).
68. G. Xie *et al.*, Local angiotensin II contributes to tumor resistance to checkpoint immunotherapy. *J. Immunother. Cancer* **6**, 88 (2018).
69. D. Fukumura, J. Kloepper, Z. Amoozgar, D. G. Duda, R. K. Jain, Enhancing cancer immunotherapy using antiangiogenics: Opportunities and challenges. *Nat. Rev. Clin. Oncol.* **15**, 325–340 (2018).
70. D. Fukumura *et al.*, Tumor induction of VEGF promoter activity in stromal cells. *Cell* **94**, 715–725 (1998).
71. Y. Hayakawa *et al.*, IFN-gamma-mediated inhibition of tumor angiogenesis by natural killer T-cell ligand, alpha-galactosylceramide. *Blood* **100**, 1728–1733 (2002).
72. M. Gordon-Alonso, T. Hirsch, C. Wildmann, P. van der Bruggen, Galectin-3 captures interferon-gamma in the tumor matrix reducing chemokine gradient production and T-cell tumor infiltration. *Nat. Commun.* **8**, 793 (2017).
73. S. Marino, I. B. Hogue, C. J. Ray, D. E. Kirschner, A methodology for performing global uncertainty and sensitivity analysis in systems biology. *J. Theor. Biol.* **254**, 178–196 (2008).
74. S. J. Conley *et al.*, Antiangiogenic agents increase breast cancer stem cells via the generation of tumor hypoxia. *Proc. Natl. Acad. Sci. U.S.A.* **109**, 2784–2789 (2012).
75. L. G. de Pillis, A. E. Radunskaya, C. L. Wiseman, A validated mathematical model of cell-mediated immune response to tumor growth. *Cancer Res.* **65**, 7950–7958 (2005).
76. M. De Palma, R. K. Jain, $CD4^+$ T cell activation and vascular normalization: Two sides of the same coin? *Immunity* **46**, 773–775 (2017).
77. J. Holash *et al.*, Vessel cooption, regression, and growth in tumors mediated by angiopoietins and VEGF. *Science* **284**, 1994–1998 (1999).
78. I. B. Lobov, P. C. Brooks, R. A. Lang, Angiopoietin-2 displays VEGF-dependent modulation of capillary structure and endothelial cell survival in vivo. *Proc. Natl. Acad. Sci. U.S.A.* **99**, 11205–11210 (2002).
79. L. Eklund, J. Kangas, P. Saharinen, Angiopoietin-Tie signalling in the cardiovascular and lymphatic systems. *Clin. Sci. (Lond.)* **131**, 87–103 (2017).
80. R. G. Akwii, M. S. Sajib, F. T. Zahra, C. M. Mikelis, Role of Angiopoietin-2 in vascular physiology and pathophysiology. *Cells* **8**, E471 (2019).
81. U. M. Domanska *et al.*, A review on CXCR4/CXCL12 axis in oncology: No place to hide. *Eur. J. Cancer* **49**, 219–230 (2013).
82. F. Mpekris, S. Angeli, A. P. Pirentis, T. Stylianopoulos, Stress-mediated progression of solid tumors: Effect of mechanical stress on tissue oxygenation, cancer cell proliferation, and drug delivery. *Biomech. Model. Mechanobiol.* **14**, 1391–1402 (2015).
83. A. S. Popel, Theory of oxygen transport to tissue. *Crit. Rev. Biomed. Eng.* **17**, 257–321 (1989).